Balmer and Metal Absorption Feature Gradients in M32

Guy Worthey

Program in Astronomy, Washington State University, Pullman, WA 99164-2814

ABSTRACT

New data sources are used to assess Lick/IDS feature strength gradients inside the half-light radius R_e of the compact Local Group elliptical galaxy M32. A *Hubble Space Telescope* (HST) STIS spectrum seemed to indicate ionized gas and a very young central stellar population. In fact, this conclusion is entirely spurious because of incomplete removal of ion hits. More robust ground-based spectra taken at the MDM Observatory are, in contrast, the most accurate measurements of Lick/IDS indices yet obtained for M32. All but a few (of 24 measured) indices show a statistically significant gradient. The CN indices show a maximum at $4''$ radius, dropping off both toward the nucleus and away from it. At $2''$ radius there is a discontinuity in the surface brightness profile, but this feature is not reflected in any spectral feature. Comparing with models, the index gradients indicate a mean age and abundance gradient in the sense that the nucleus is a factor of 2.5 younger and a factor of 0.3 dex more metal-rich than at 1 R_e. This conclusion is only weakly dependent on which index combinations are used and is robust to high accuracy. Stars near the M32 nucleus have a mean age and heavy element abundance [M/H] of (4.7 Gyr, +0.02), judging from models by Worthey with variable abundance ratios. This result has very small formal random errors, although, of course, there is significant age-metallicity degeneracy along an (age, abundance) line segment from (5.0 Gyr, 0.00) to (4.5 Gyr, +0.05). An abundance pattern of [C/M]= +0.077 (carbon abundance affects CN, $C_2$4668, and the bluer Balmer features), [N/M]= −0.13, [Mg/M]= −0.18, [Fe/M]≈0.0, and [Na/M]= +0.12 is required to fit the feature data, with a fitting precision of about 0.01 dex (with two caveats: the [Fe/M] guess has about twice this precision because of the relative insensitivity of the Fe5335 feature to iron, and the [Na/M] value may be falsely amplified because of interstellar absorption). Model uncertainties make the accuracies of these values at least twice the magnitude of the precision. Forcing scaled-solar abundances does not change the age very much, but it increases the rms goodness of model-data fit by a factor of 3 and broadens the allowed range of age to ±1 Gyr. The abundance ratios do not show strong trends with radius, except for the nuclear weakening of CN (measuring mainly N) mentioned above, which needs reconfirming with better data. The overall abundance pattern contrasts with larger elliptical galaxies, in which all measurable lighter elements are enhanced relative to iron and calcium. Nucleosynthetic theory does not provide a ready explanation for these mixtures.

Subject headings: galaxies: stellar content — galaxies: individual (M32) — galaxies: elliptical and lenticular, cD — galaxies: abundances — galaxies: fundamental parameters

1. Introduction

M32 is a compact elliptical galaxy of around $10^9 M_\odot$ southeast of the nucleus of the Andromeda galaxy. It shares the distinction of being the nearest elliptical galaxy with NGC 205, Andromeda's other elliptical companion. Structurally, M32 lies near an extrapolation of elliptical galaxy properties, whereas NGC 205, with its much lower surface brightness, has more in common with disk galaxies (Kormendy 1989). It is usually M32, therefore, that attracts attention from those interested in the properties, histories, and stellar populations of elliptical galaxies. Enthusiasm should be tempered by some caution since M32 is so dense that analogues are rare, and so it may represent a subclass of elliptical galaxies rather than elliptical galaxies in general. It probably contains a central black hole of mass 3×10^6 $M_\odot$ (Bender et al. 1996).

A comprehensive understanding of M32's history would connect its structure and kinematics with its stellar population properties. There is some dispute in the literature, but most investigations agree that the nuclear regions of M32 are best fit with a stellar population of approximately solar composition and an age of, very roughly, 4 Gyr. Published long-slit spectroscopy of M32 (González 1993, hereafter G93) does not reach as far as $1\farcm3$ [1.8 R_e(PA); 66% of light enclosed] from the nucleus where *Hubble Space Telescope* (HST) photometry of resolved red giants was obtained by Grillmair et al. (1996). Under the assumption of constant age the colors of the giants map uniquely to abundance, and the abundance spread found is very similar to that of the solar neighborhood. The best consistency with *extrapolated* G93 spectroscopy was obtained with old ages of 8 Gyr or older. It should be emphasized that the models simultaneously matched both the distribution of giant temperatures and all spectroscopic indices.

Only G93 gives a suitable comparable data set for optical feature-strength gradients on the Lick/IDS system [system definition in Worthey et al. (1994); Worthey & Ottaviani (1997)]. Hardy et al. (1994) gave long-slit data for M32 but did not transform completely to the Lick/IDS system. Davidge (1991) measured eight high-quality indices, but his spectra apparently had a spectral resolution somewhat coarser than Lick/IDS, as evidenced by the fact that the narrower indices were weaker in comparison stars. This data could, in principle, be linearly transformed to the Lick/IDS system, but this has not been attempted here. The Davidge (1991) results do make a very useful near-differential comparison set, and we agree with his conclusion that most spectral indices show gradients in the central $20''$. Jones & Rose (1994) report that no index gradients are observed in the central $30''$ but give no further information. High-quality nuclear and near-nuclear data are given in Trager et al. (1998), del Burgo et al. (2001), and Rose (1994). This short

paper summarizes additional ground-based (MDM) and space-based (HST) long-slit spectra. The HST *Space Telescope Imaging Spectrograph* (STIS) spectra are discussed in §2, followed by the ground-based data.

2. Spectra from Space and False Conclusions

The light profile of M32 (Figure 1) is strongly suggestive of two components: a compact, dense nuclear component superposed on a broader, nearly $r^{1/4}$ profile. The inner two arcseconds, about 7 parsecs in radius, almost look like a distinct subgalaxy in the light profile. It behooves the investigator to look for stellar population differences at this radius. Kinematic and structural discontinuities in elliptical galaxies are often marked by changes in the slopes of absorption feature-strength gradients at the corresponding location (Bender & Surma 1992).

The HST STIS data were obtained on 1999 August 6 for program 7438 proposed by R. W. O'Connell and others [cf. O'Connell et al. (2000)]. The bulk of the exposure time was spent on the ultraviolet portion of the spectrum, but two exposures (2490 and 3000 s) through a $52''$ by $0\farcs2$ slit were taken with the optical CCD and the G430L disperser. The dispersion (2.7 Åpixel^{-1}) is perfectly adequate for the measurement of Lick/IDS indices. The excellent spatial resolution implies many resolution elements within the $2''$ central component seen in the light profile.

Since it turned out to be impossible to measure accurate spectral indices with this data set, I wish to be brief. After pipeline calibration and (partial) rejection of cosmic rays through image combination, spectra were traced, extracted, and wavelength-calibrated through a cross-correlation technique. Lick/IDS indices were measured at 1 pixel intervals along the slit. The result is displayed in Figure 2 for several Balmer indices. The false positive indication of ionized gas plus young stars in the inner $2''$ appears to be due entirely to residual cosmic-ray blemishes that were either too subtle to be removed or appeared on both available images. The reasons for this conclusion are that (1) other indices show spikes or dips at different, apparently random radii; (2) observations symmetric about the center trace are often quite different; and (3) the large range of data (e.g., -2 to 8 Å for Hβ) does not square with ground-based results, in which Hβ lies between 1.9 and 2.3 Å over the whole range of radii. It is interesting to note that the total exposure time of the optical STIS spectra is roughly the same as the sum of the exposures described below through a telescope of the same aperture, but the errors are at least an order of magnitude higher.

3. Spectra from the Ground

3.1. Observations

Ground-based long-slit spectra of M32 suitable for Lick/IDS index analysis were obtained at the MDM Observatory 2.4 m telescope during three runs: 1993 September, 1994 October, and 1997

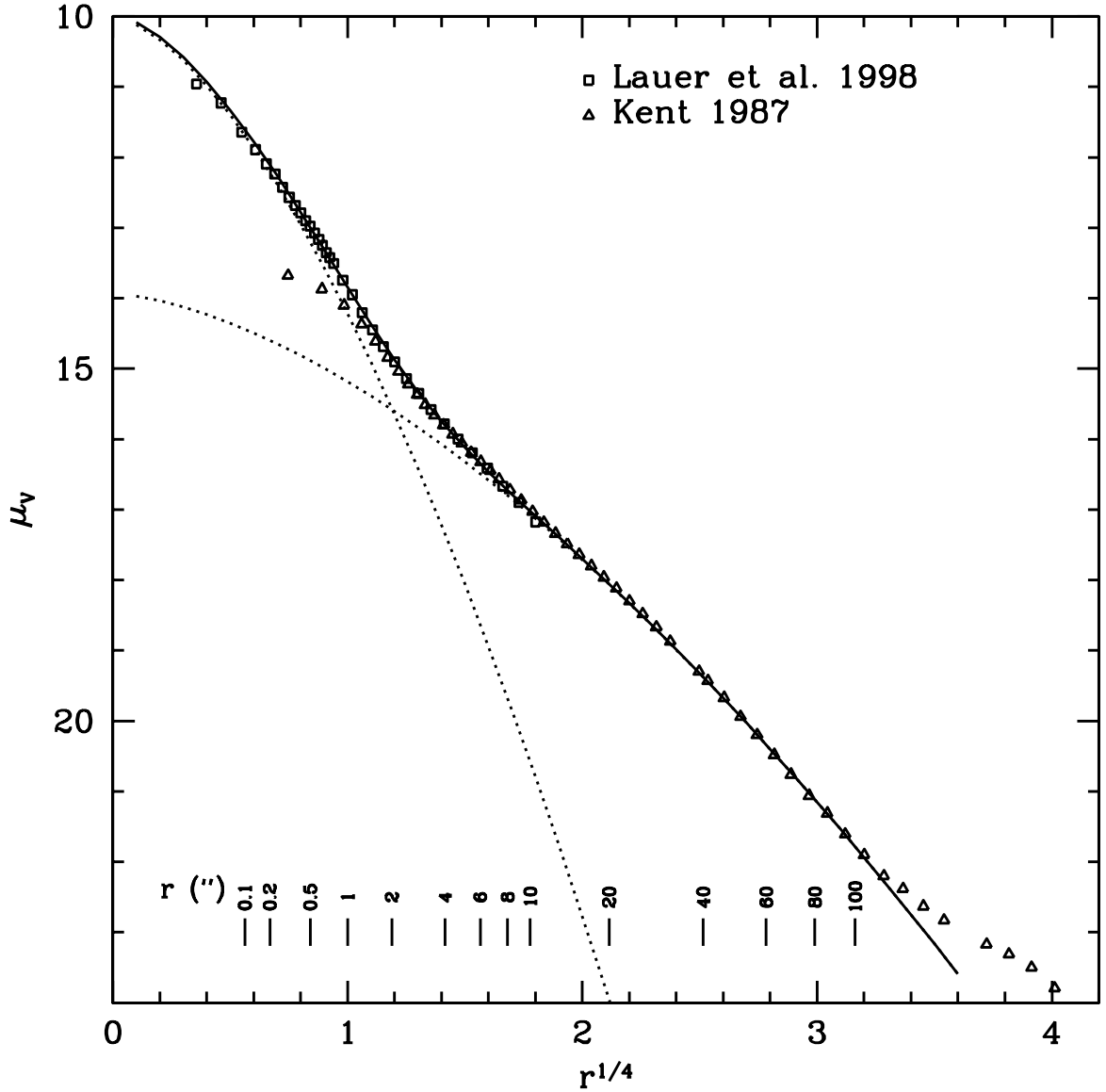

Fig. 1.— Light profile of M32 from Lauer et al. (1998) for the inner portions and Kent (1987) for the outer portions. A shift of 0.35 mag was applied to the Kent data to transform it to V magnitude. Two Sérsic functions (*dotted lines*) and their sum (*solid line*) are plotted, indicating a structural discontinuity at around $r = 2''$. The spatial scale is 3.7 pc arcsecond^{-1}.

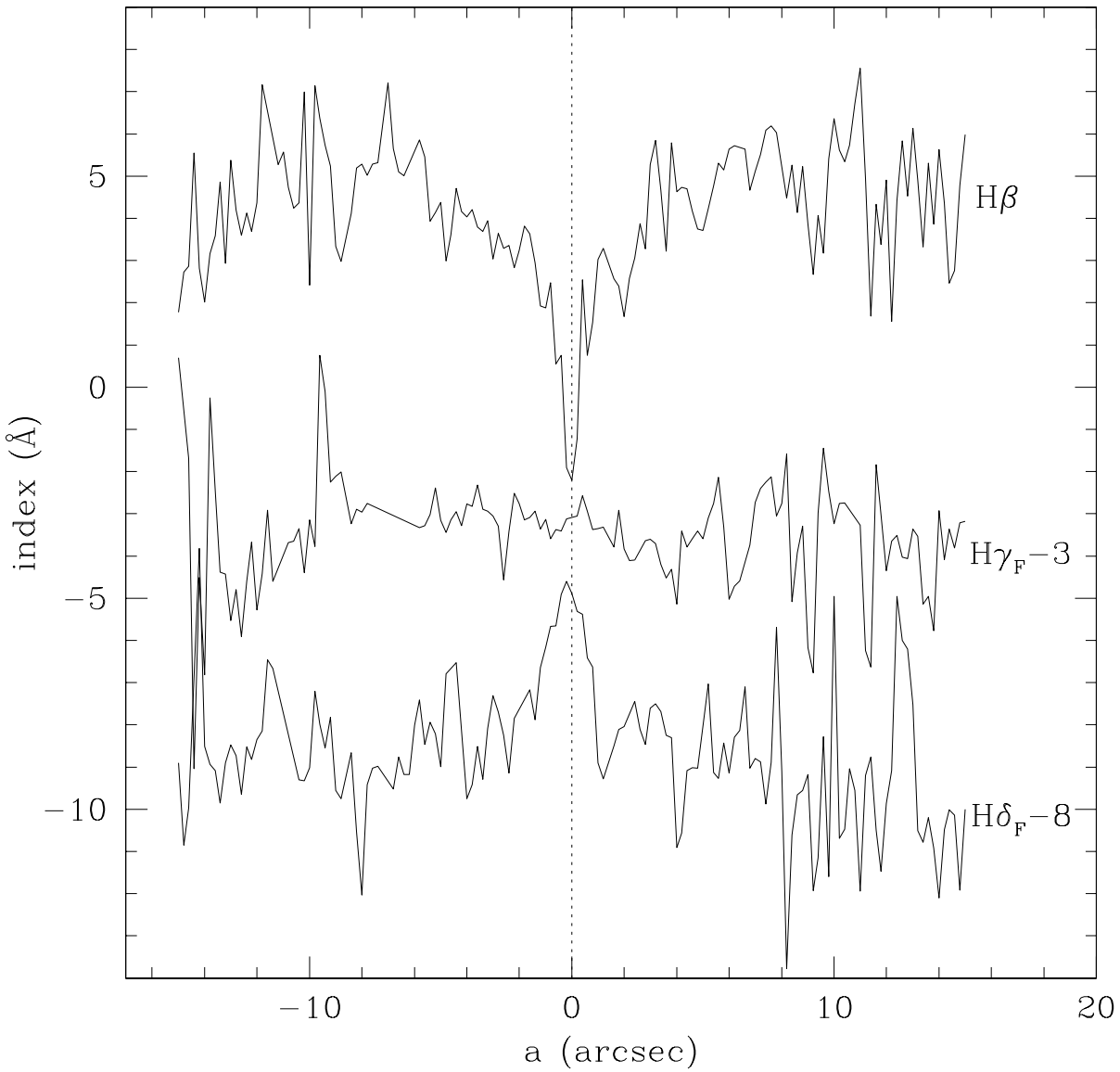

Fig. 2.— Radial profiles for Lick Balmer indices in M32 as a function of distance along the slit. The nucleus is at zero. The qualitative appearance of these three Balmer indices suggests a pattern of hydrogen emission plus young stars near the nucleus, with Hβ negative (as expected for emission), Hγ flat, and Hδ positive (as expected for young stars). Appearances are deceiving in this case, because this pattern is entirely an artifact of residual cosmic-ray noise in the STIS spectra that just happens, in this case, to look plausibly astrophysical, at just the scale predicted by the surface brightness profile.

June. The Mark 3 spectrograph was used with blue-sensitive chips ("Charlotte" in 1993 and 1994 and "Templeton" in 1997), with wavelength coverage from about 3800 to 6100 Å at 2.3 Å pixel^{-1} dispersion. The resolution was a function of wavelength and run but was always less than Lick/IDS and therefore easily transformable to the Lick/IDS system given the nightly set of standard stars observed. Both chips had the same pixel size, so the spatial scale was constant at $0\farcs78$ pixel^{-1}. The M32 spectra were obtained with the slit oriented north-south. This is 10° away from the major axis of the galaxy [PA = 170°; de Vaucouleurs et al. (1991)] but amounts to a foreshortening of only 1%, which is less than the uncertainty in the spatial scale.

Three exposures in 1993, three in 1994, and four in 1997, with exposure times ranging from 600 to 1200 s, were bias-subtracted and flat-fielded using IRAF tasks. Only the 1994 exposures were sufficiently homogeneous to be co-added. This was done, and we analyzed the median image in conjunction with the others. The sky was sampled more than $100''$ away and was dominated by terrestrial sky rather than galaxy light. The galaxy fades by factors of $15-40$ from the last extracted spectra at $55''$ to where the sky was sampled. Indices are affected by such self-subtraction in second order. For example, if the $55''$ measurement of Hβ is 2.0 Å but the sky region of M32 has Hβ = 1.5 Å, the $55''$ measurement will be decreased by, at most, $(2.0 - 1.5)/15 = 0.03$ Å. If the sky has the same index value as the target region, no change will result. Other defects were present in some images. Two images had saturated pixels near the nucleus, three suffered a sky oversubtraction problem during processing that had to be corrected by hand, and all images had a fair number of cosmic ray tracks except for the one median-combined image from 1994. Seventy 1 pixel wide spectra were extracted from each side of the nucleus, plus 1 central pixel. These were cross-correlated with synthetic stellar templates to put them on a zero-velocity wavelength scale.

Lick/IDS indices were measured from each spectrum. Each index had 11 independent measurements at each slit location, so with symmetric north-south pairs analyzed together, all radii except the central pixel had 22 measurements. The expectation was that most indices would cluster around the true index value, but some would be affected by a cosmic ray and would be very wild. The median was therefore adopted as the statistic of choice. The error was computed by bootstrap resampling. The complete table of median index values and errors shown in Fig 3 is available from the author. Note that the index TiO_2 is not included because it falls past the red end of the MDM spectra.

Figure 3 shows the main gradient results, compared with nuclear values from the original Lick/IDS data set and also G93 for overlapping indices. A polynomial-smoothed version of the index results is plotted as a line and also presented in Table 1. The errors listed below the index entries in Table 1 are indicative errors for the sum of data points near each tabulated radius. That is to say, they are larger than the formal error from the curve fit. It was thought that the data-based error was more appropriate since many curves could be fit, giving a spread of results despite formally small errors. Table 2 weights the Table 1 results by surface brightness and radius to simulate the index value measured inside a circular aperture. The last entry in Table 2 is an extrapolation to two effective radii, or about 69% of light enclosed assuming an $r^{1/4}$ exponential

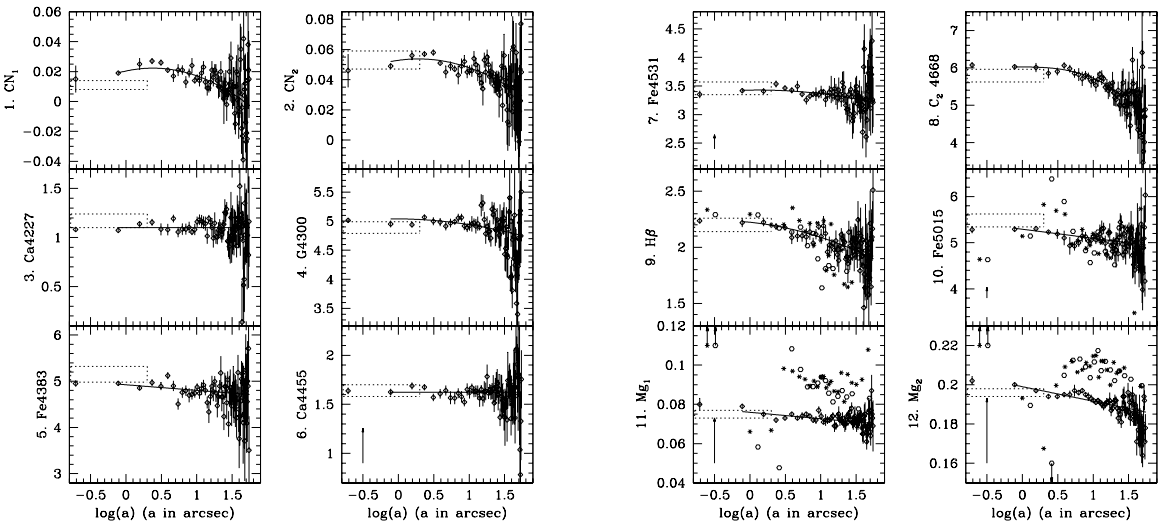

Fig. 3.— Plots of median index values from the MDM data (*diamonds*) and their errors as a function of the logarithm of the semimajor axis of the isophotal ellipse on which each sampled spectrum lies. The curve segments are least-square fits to the data. If there was a non-negligible correction for systematics, the applied correction is plotted as a vertical arrow at $\log(a) = -0.5$. Nuclear Lick/IDS measurements from Trager et al. (1998) (or, in the case of Hγ and Hδ, unpublished) are indicated as dotted boxes that end at the nominal Lick/IDS slit length of $4''/2 = 2''$ radius. The boxes enclose $\pm 1\sigma$. If G93 values exist, they are plotted as asterisks (*major axis*) or open hexagons (*minor axis*) with error bars suppressed. A few G93 data points are indicated as upper or lower limits if they fall outside the region plotted.

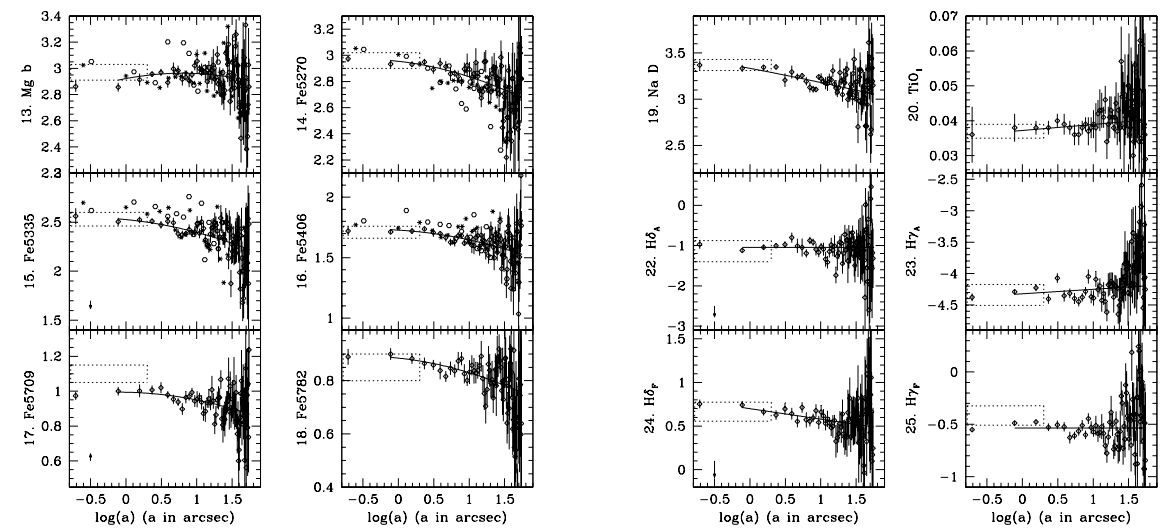

Fig. 3.— This is a continuation of Figure 3.

profile.

Comparing indices in common with G93, we note that, as G93 predicted because of a chromatic focus problem and night-sky lines at Lick Observatory, Fe5015, Mg_1, and Mg_2 drift quite a lot. Other indices match well, except for Mg b, discussed immediately below. Gradient strengths match between the data sets except for Hβ and Fe5270, for which we obtain shallower slopes.

Fits to all of the data with lines indicate, via the F-test, that Ca4227, Ca4455, Hδ_A, and Hγ_F are statistically consistent with a value that is constant rather than sloped with radius. Fits to higher order polynomials indicate, even for these four, statistically better fits at higher order. However, I decided against polynomials more complicated than a quadratic to model the radial trends (except $C_2$4668, for which a cubic was irresistible). Note that the fact that I find few constant indices is not inconsistent with del Burgo et al. (2001), who detected no radial gradients in any index, since their data go to a radius of $5''$, equivalent to the first six points in Figure 3, and with larger errors. Over this spatial range, only the CN indices show a strong deviation from constant behavior. There is no hint that any stellar population feature manifests itself at the $2''$ discontinuity in the surface brightness profile.

The near-nuclear drop of the CN indices is surprising, given the lack of any such feature in any other index, and it may or may not be real. If it is due mostly to a drop in N abundance, then the violet NH feature gradient data of Davidge et al. (1990) provides support for its reality since this gradient is also negative. However, whereas the present data set turns over at 4-5 arcsec, the Davidge et al. (1990) data keep climbing to the limit of their data at $\approx 11''$. Flattening is possible, given the error bars, so the two data sets may agree. Alternatively, future modeling may indicate that age effects dominate over abundance effects for the NH index, and in that case we should expect it to weaken toward the nucleus from straightforward age gradient effects. Clearly, this issue is one that should be resolved with further observation.

Greater than 1 σ zero-point discrepancies occur between this data set and the original Lick/IDS M32 nuclear data for indices Mg b and Fe5709. Indices Mg_1, Mg_2, and Na D also were initially somewhat discrepant, but a second analysis pass modified the systematic corrections (based on stars and represented by arrows in Figure 3) that were applied. The relatively large corrections for Mg_1 and Mg_2 are expected because they are very broad and subject to the effects of instrumental response more than other indices. Of the persistently discrepant indices Fe5709 has no measurements from other sources besides Lick/IDS, so it is hard to assess which data source might be in error.

The Mg b index, however, may be in some trouble. It is ~ 2 σ weaker than the measurement of G93, ~ 1.5 σ weaker than Lick/IDS, and ~ 1 σ weaker than del Burgo et al. (2001). However, it is essentially identical to the values in Figure 9 of Kormendy & Bender (1999). In stellar comparisons the Mg b index was consistent with no systematic drift at all. Additionally, the sense of the MDM Mg b gradient in the inner few pixels is opposite that of G93 and also opposite that of Mg_1 and Mg_2. It is possible that the MDM data underestimate Mg b by about 0.1 Å in the inner 2 pixels,

or $1\farcs6$, but not certain.

A large systematic correction was applied to Ca4455 on the basis of stellar comparisons. This correction was similar for all three data sets and appears to be a real shift between the original and the MDM systems. Its origin is unknown.

3.2. Mean Age

The basic technique of arriving at a mean-age, mean-abundance pair using Lick/IDS indices was articulated by Worthey (1994) and expanded on by many authors, among them del Burgo et al. (2001), Trager et al. (2000), Tantalo et al. (1998), and Thomas & Maraston (2003). An unofficial median of ages quoted for the stellar population in the nucleus of M32, including other methods of spectral comparison (e.g. O'Connell (1980), Rose (1994), Bica, Alloin, & Schmidt (1990), and Vazdekis & Arimoto (1999)), is around 4 Gyr. Quoting a mean age does not, of course, mean that M32 sprang into existence 4 Gyr ago. Galaxies are complex systems with considerable chemodynamic history behind them and we should expect abundance distributions (probably fairly regular) and age distributions (probably irregular) for them. The mean age and abundance are nevertheless convenient signposts, at least for statistical studies.

Effects that would strengthen Balmer-line strengths by adding warm or hot stars, such as unexpected horizontal-branch morphology or blue straggler stars, are conveniently muted in M32 compared with large, redder elliptical galaxies: regarding extreme horizontal-branch star contributions, Burstein et al. (1988) find that M32 has the least mid-UV flux of any galaxy in their sample, and Rose (1994) finds that an intermediate-age population plus a frosting of metal-poor stars accounts for all of the observables available to him at high spectral resolution. Furthermore, G93 found negligible nebular emission in M32. Again, M32 seems safe because its Balmer lines are already strong, so any possible emission line spectrum would have to be fairly powerful to affect our interpretation. Finally, nonsolar abundance ratio effects are mild in M32 (see below). This greatly reduces the danger of significant modulations of either the main-sequence turnoff temperature or the giant branch temperature, the two quantities fundamentally measured by the Balmer-metal technique, as a result of altered chemical mixtures causing changes in the structures of the stars.

Some Balmer-metal diagrams are shown in Figure 4, using Hβ as an example. Use of the other four Balmer indices gives virtually identical results. What Figure 4 shows is that (1) inferred age depends on which metal feature is used. Mg_2 and Fe5335 give ages of around 4 Gyr whereas Fe5270 and $C_2$4668 yield ages closer to 2.5 Gyr. (2) Inferred abundance also shifts. (3) Age increases and abundance drops with radius. In this case the changes are very similar from diagram to diagram, with the abundance always ranging somewhat more than one 0.25 dex interval, and the age spanning factors of 2.5−3 from the nucleus to the last measured point at 1 R_e.

The shifts from panel to panel in Figure 4 are due to abundance ratio changes, discussed more

Table 1. Polynomial-Smoothed Indices and Errors

a (arcsec)	CN_1	CN_2	Ca4227	G4300	Fe4383	Ca4455	Fe4531	$C_2$4668	Hβ	Fe5015	Mg_1	Mg_2
0.195	0.015	0.046	1.101	5.002	5.010	1.624	3.371	6.075	2.234	5.431	0.078	0.204
	0.009	0.012	0.015	0.021	0.062	0.032	0.067	0.076	0.026	0.074	0.003	0.005
0.78	0.019	0.052	1.101	5.039	4.937	1.624	3.424	6.024	2.230	5.313	0.076	0.200
	0.001	0.002	0.014	0.057	0.049	0.035	0.043	0.041	0.040	0.058	0.001	0.001
1.56	0.022	0.054	1.101	5.034	4.901	1.624	3.428	6.018	2.208	5.254	0.075	0.198
	0.004	0.003	0.025	0.042	0.044	0.038	0.047	0.125	0.034	0.029	0.001	0.001
2.34	0.022	0.054	1.101	5.023	4.879	1.624	3.424	5.999	2.190	5.219	0.075	0.196
	0.002	0.002	0.032	0.050	0.073	0.032	0.060	0.142	0.030	0.028	0.001	0.001
4.0	0.022	0.053	1.101	5.001	4.851	1.624	3.410	5.944	2.159	5.173	0.074	0.195
	0.001	0.002	0.035	0.052	0.066	0.035	0.054	0.066	0.038	0.126	0.001	0.001
6.5	0.020	0.051	1.101	4.972	4.825	1.624	3.390	5.850	2.125	5.132	0.073	0.193
	0.002	0.002	0.027	0.032	0.063	0.031	0.030	0.073	0.031	0.052	0.001	0.001
10	0.017	0.048	1.101	4.940	4.803	1.624	3.366	5.722	2.089	5.095	0.073	0.192
	0.001	0.002	0.021	0.038	0.045	0.022	0.038	0.058	0.023	0.045	0.001	0.001
15	0.014	0.045	1.101	4.904	4.781	1.624	3.338	5.554	2.051	5.061	0.072	0.190
	0.002	0.002	0.025	0.049	0.061	0.027	0.054	0.065	0.027	0.049	0.001	0.001
25	0.008	0.040	1.101	4.851	4.754	1.624	3.296	5.268	1.996	5.017	0.071	0.189
	0.002	0.002	0.034	0.054	0.072	0.035	0.049	0.081	0.029	0.050	0.001	0.001
40	0.002	0.034	1.101	4.794	4.730	1.624	3.250	4.917	1.940	4.977	0.071	0.187
	0.003	0.004	0.046	0.084	0.105	0.050	0.066	0.110	0.037	0.077	0.001	0.001
a (arcsec)	Mg b	Fe5270	Fe5335	Fe5406	Fe5709	Fe5782	Na D	TiO_1	Hδ_A	Hγ_A	Hδ_F	Hγ_F
0.195	2.861	2.968	2.546	1.730	0.981	0.891	3.369	0.036	-1.043	-4.373	0.785	-0.535
	0.040	0.021	0.088	0.039	0.016	0.030	0.047	0.008	0.098	0.062	0.044	0.015
0.78	2.910	2.960	2.533	1.731	0.994	0.887	3.349	0.037	-1.043	-4.329	0.713	-0.535
	0.036	0.037	0.041	0.020	0.025	0.022	0.037	0.003	0.057	0.045	0.036	0.025
1.56	2.939	2.940	2.510	1.719	0.991	0.878	3.306	0.038	-1.043	-4.308	0.676	-0.535
	0.048	0.020	0.032	0.021	0.038	0.021	0.025	0.002	0.061	0.051	0.045	0.021
2.34	2.951	2.924	2.492	1.709	0.986	0.871	3.279	0.038	-1.043	-4.295	0.655	-0.535
	0.017	0.023	0.025	0.013	0.027	0.022	0.027	0.002	0.054	0.075	0.050	0.037
4.0	2.960	2.897	2.462	1.690	0.976	0.858	3.244	0.038	-1.043	-4.278	0.627	-0.535
	0.031	0.030	0.032	0.018	0.017	0.019	0.039	0.002	0.108	0.059	0.047	0.035
6.5	2.963	2.867	2.429	1.669	0.963	0.844	3.211	0.039	-1.043	-4.263	0.602	-0.535
	0.020	0.020	0.020	0.015	0.014	0.014	0.020	0.001	0.064	0.038	0.033	0.022
10	2.960	2.837	2.395	1.647	0.950	0.830	3.180	0.039	-1.043	-4.250	0.579	-0.535
	0.017	0.030	0.022	0.018	0.015	0.016	0.019	0.002	0.060	0.047	0.032	0.026
15	2.954	2.804	2.360	1.623	0.934	0.815	3.152	0.039	-1.043	-4.237	0.558	-0.535
	0.026	0.024	0.028	0.021	0.017	0.018	0.023	0.001	0.068	0.058	0.041	0.034
25	2.940	2.758	2.309	1.589	0.911	0.793	3.114	0.040	-1.043	-4.221	0.532	-0.535
	0.026	0.028	0.031	0.024	0.021	0.018	0.026	0.002	0.091	0.083	0.058	0.039
40	2.921	2.711	2.258	1.554	0.887	0.771	3.079	0.040	-1.043	-4.206	0.507	-0.535
	0.036	0.042	0.045	0.032	0.028	0.029	0.040	0.003	0.131	0.100	0.077	0.054

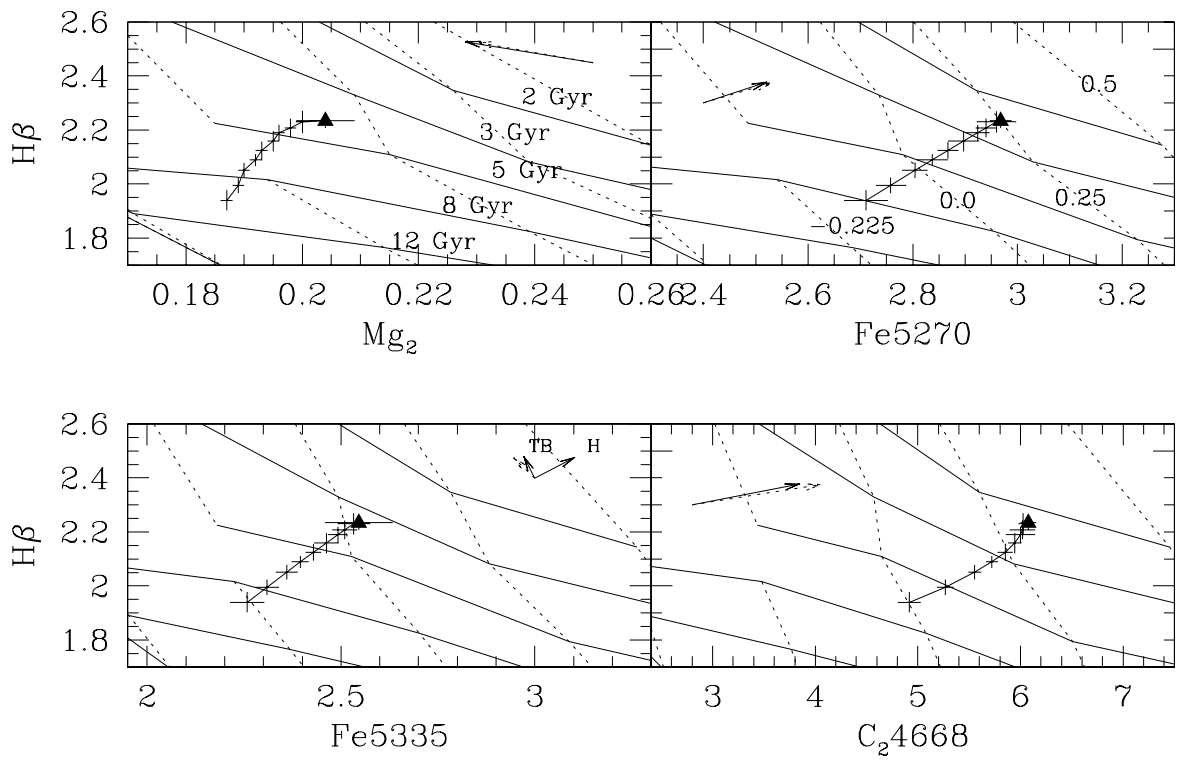

Fig. 4.— Plots of four age-metal diagnostic diagrams that array Hβ against metal features. M32 spectral data from Table 1 are plotted, with the central pixel marked as a triangle and subsequent samples marked only by error bars. Worthey (1994) models are plotted as a grid with same-age lines plotted with solid lines and same-abundance lines plotted with dotted lines. The ages are marked in the Mg_2 panel, and the [M/H] values are marked in the Fe5270 panel. The vectors drawn with dotted lines represent the vector between the model for (age, [M/H]) = (4.75 Gyr, 0.02) and the table 2 nuclear-aperture observation. The vectors drawn with solid lines represent a model shift caused by the slightly nonsolar abundance pattern that is discussed in the next section. The "TB" and "H" choices in the Fe5335 panel stand for predictions based on TB95 and Houdashelt et al. (2002) synthetic stellar fluxes. The Houdashelt et al. (2002) fluxes were used for all other panels.

fully in the next section. The younger ages in the Fe5270 and $C_2$4668 panels are due to increased index strength due to enhanced carbon, so the older ages are the more reliable in this case. This is tempered by uncertainty in oxygen abundance, which we do not yet measure, but which can effect changes in isochrone shape [cf. Worthey (1998)]. Forcing adherence to scaled-solar index models, 4 Gyr would be our best guess with the current data and models for the nucleus, with a mean abundance just slightly more than solar, say +0.05. This quickly fades with radius to 8-10 Gyr age and abundance of -0.25 for a radius of 1 $R_e = 44\farcs4$ along the major axis, or 164 pc from the nucleus. The corresponding minor axis distance would be $34\farcs2$, or 127 parsec.

The age and metal abundance hover around those discussed in Grillmair et al. (1996) for their HST field at 1.8 R_e. The Lick indices extrapolated from G93 data indicated age and abundance of (8.5 Gyr, -0.25). Our data would extrapolate to older and slightly more metal-poor, about (10-11 Gyr, -0.35) using the [MgFe] composite index. From the Grillmair et al. (1996) photometry, and assuming 10 Gyr isochrones, the $V - I_C$ colors of the giants indicate a peak abundance of -0.2. Realizing that the metal-poor side of this peak will contribute somewhat more than the metal-rich side to the spectroscopic mean age via greater luminosity and greater contribution to Balmer strengths, the two approaches are probably still fairly closely in harmony with each other, although a detailed revisit to the problem would be a good idea. The older extrapolated age from the new spectroscopy is something of a surprise since the new Hβ gradient is shallower than G93, but other small changes, such as a shallower Fe5270 gradient and a depressed Mg b index, compensate for this.

3.3. Abundance Ratios

A discussion of abundance ratio patterns in early-type galaxies is found in Worthey (1998). The major trend is that larger elliptical galaxies have deviations from scaled-solar ratios in the sense that light elements are enhanced relative to Fe-peak elements. Since not every light element can presently be measured, this is partly an assumption based on yield predictions from Type Ia and Type II supernovae. Low-mass elliptical galaxies, like M32, have nearly solar element ratios.

Diagrams that plot metal index against metal index are usually highly degenerate with respect to age and scaled-abundance changes. This leaves such diagrams sensitive to changes that are not simply different combinations of age and metallicity, namely the modulation of abundance ratios, such as [Mg/Fe] [cf. the "age-metallicity degeneracy" and "theorem of sensitivity" of Worthey (1994)]. Models that track many abundance mixtures with perfect self-consistency (meaning that all ingredients from opacities to stellar isochrones to stellar fluxes would be produced with the same element mixtures) have not yet been produced, but brave forays in this direction have been made (Trager et al. 2000; Thomas, Maraston, & Bender 2003). For this paper we stay with the scaled-solar models of Worthey (1994), augmented by the calculations of nonsolar-mixture synthetic stellar calculations of Houdashelt et al. (2002), which are very similar to those of Tripicco & Bell (1995) (hereafter TB95).

An issue uncovered with the TB95 synthetic fluxes should be mentioned here. Their carbon enhancement was 0.3 dex, sufficient to make the number abundance of carbon exceed that of oxygen. The large dissociation energy of the CO molecule causes most of the carbon to be locked up in this molecule in oxygen-rich stars, but in carbon-rich stars C_2 Swan bands begin to dominate the visible spectrum in a nonlinear way, approximately as the square of the carbon abundance. The responses for carbon in TB95's tables 4, 5, and 6 are therefore significantly overestimated. We double checked this conclusion with sets of synthetic spectra kindly provided by A. Korn, by M. Briley, and also by E. Baron. The Houdashelt et al. (2002) carbon responses were computed with a carbon enhancement of 0.15 dex and thus do not change the molecular equilibrium very much.

In galaxy data like those considered here, abundance ratios can be estimated from scaled-solar models by assuming that any deviation between the model and the observations results from an individual element enhancement that acts like an overall abundance increase, as seen, for instance, in Worthey, Faber, & González (1992). This works only roughly, as (1) the Lick/IDS indices cover many blended lines and therefore other species besides the dominant one contribute and (2) abundance mixture changes the underlying isochrone. Trager et al. (2000) and Thomas, Maraston, & Bender (2003) effectively calibrate against line blends by using the results of TB95, who explored the effects of element ratio changes in the spectra of three representative stars. The approach taken here is essentially the same as Trager et al. (2000) and Thomas, Maraston, & Bender (2003), except that we use Houdashelt et al. (2002) spectra.

Using the rms fit of model versus data (the Table 2 nuclear data point) as a figure of merit, a best-fit age, overall "metallicity" [M/H], and abundance mixture were found. The best age is 4.75 Gyr, with [M/H]=+0.02. Small abundance changes were sought simultaneously to improve the fit. The primary ones are [C/M]=+0.077, [N/M]=−0.13, [Mg/M]=−0.18, and [Na/M]=+0.12. These are relatively well measured, since they affect a variety of indices in a substantial way. The sodium abundance, of course, could be spurious because of interstellar absorption in the Na D feature, but the other measurements are good to roughly 0.02 dex, for which most of the uncertainty is in the models, not the data. Elements with much larger uncertainty because of the fact that they do not strongly impact the Lick/IDS indices are [O/M]=[Fe/M]=[Ca/M]=[Si/M]$\approx$ 0, [Cr/M]≈ -0.15, and [Ti/M]≈ -0.2. The indices that were used to find this solution (CN_2, Ca4227, Fe4383, $C_2$4668, Mg_2, Fe5270, Fe5335, Fe5406, Fe5709, Na D, and all five Balmer indices) had a final rms fit of 0.26 in units of the Worthey et al. (1994) standard Lick/IDS errors. Including all indices raises the rms fit to 0.43, in which the worst-fitting ones were Mg_1 and TiO_1. Both of these indices are sensitive to M giant numbers and temperatures and therefore suffer increased model uncertainty. This gives a preliminary and rough guess as to the ultimate accuracy of the Worthey (1994) models of better than half of a Lick/IDS σ. This is extremely encouraging. However, expressed in units of the accuracy of the present set of M32 *data*, the rms of 0.43 becomes 3.8. That is, the data far outstrip today's models in potential accuracy.

We illustrate the results by making a series of plots, shown in Figures 5, 6, 7, 8, and 9. The vectors drawn in the plots indicate the extent to which the abundance ratio changes are needed to

find a single mean age for M32. The dotted vector is the displacement from the Table 2 nuclear observation and the adopted (age=4.75 Gyr, [M/H]=0.02) model. The solid vector indicates the model displacement if the abundance pattern of the previous paragraph is adopted. The usually good agreement of the two vectors indicates that a single mean age plus the adopted abundance pattern fits all indices to 0.43 $\sigma_{\rm IDS}$. This reduces the age scatter from the various index-index diagrams from several gigayears to about $\pm$0.25 Gyr along an (age, abundance) line segment from (5.0 Gyr, 0.00) to (4.5 Gyr, 0.05). This is an acceptable range, not a Gaussian σ.

Figure 5 shows indices CN_2 (C- and N-sensitive), $C_2$4668 (C-sensitive), and Na D (Na-sensitive, and also sensitive to interstellar absorption). CN_2 is high because of C, and N contributes negatively. CN_2, as we have seen, has an interesting near-nuclear dip so that the nucleus approaches the space between 3 and 5 Gyr marked by the models (landing in that spot would indicate solar ratios). The inner $\sim$ 10 pc appear to have less N than the bulk of the galaxy. Before we get too excited, a lot of the signal goes away if the central pixel is omitted, and the central point has atypically large errors. A prudent scientist should not generate paragraphs of speculation based on 1 pixel. I therefore resist the temptation to write of the possible influence of a central black hole on N-rich ejecta of intermediate-mass AGB stars.

With the possible exception of nuclear N, the gradients follow the overall age-metallicity trends sketched by the model grid. This is also typical of Mg versus Fe [Figure 6 and Worthey (1998)]. This simply means that the altered abundance ratios are approximately global within the galaxy and more global than the age gradients and overall abundance gradients.

Figure 7 shows additional Fe-Fe plots. Most of the amplitude of the abundance vectors in these plots is caused by the increase in C abundance. The Fe5335 prediction from Houdashelt et al. (2002) models is quite different from that predicted by TB95. It is of much interest to pursue the cause of this discrepancy, but at the moment it is unknown and serves to indicate the extent to which it is difficult to model Lick/IDS indices in synthetic spectra. Figure 8 shows indices affected by elements N, C, and Na. With Na D, there is an observational danger in that the Kitt Peak sky contains Na D emission, so that Na D measurements in the faint parts of the galaxy may suffer from sky-subtraction problems. I mention this because, alone of the indices discussed, Na D fails to span the full range of 0.25 dex from nucleus to 1 R_e. Figure 9 shows indices that were not fitted to the abundance pattern.

4. Summary

Because of its high surface brightness, its proximity, the availability of stellar photometry in the outer parts, and its near-solar abundance ratios, M32 is an excellent laboratory for testing stellar population theory and honing integrated light models. In this paper I consider and discard the only long-slit HST STIS spectra available because it proved impossible to clean enough cosmic-ray hits from the images. Ground-based spectra from the MDM Observatory, on the other hand,

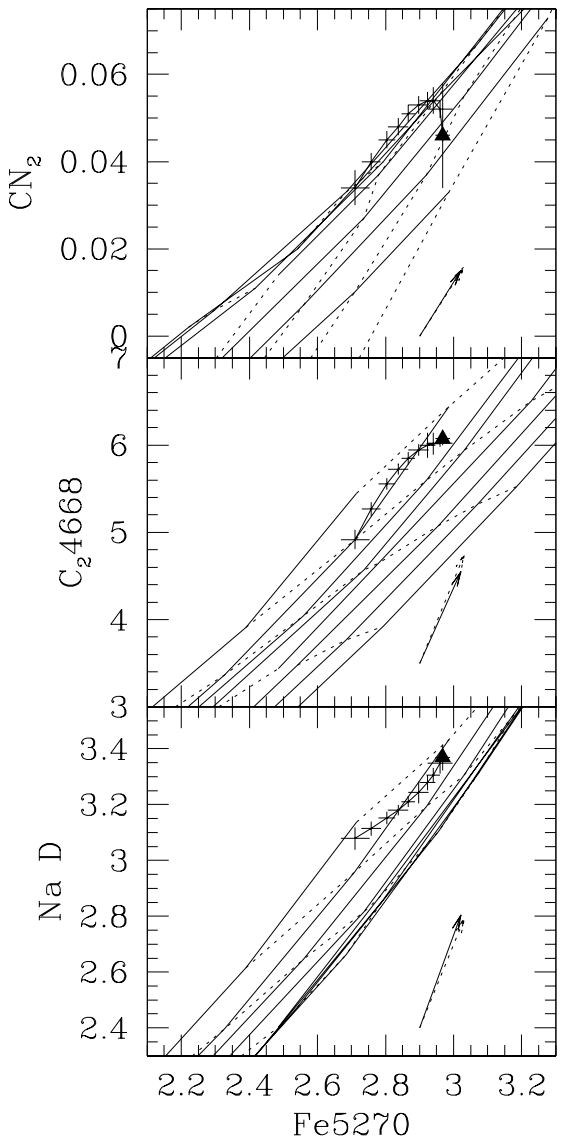

Fig. 5.— Index-index plots of abundance ratio effects in M32. Symbols are as in Figure 4: *triangle*, nucleus; *error bars*, other samples; *grid*, models. Model ages (*solid lines*) are 1, 1.5, 2, 3, 5, 8, 12, and 17 Gyr, and the top four [M/H] values (*dotted lines*) are −0.25, 0, 0.25 and 0.5. Increasing age or metallicity increases metallic feature strengths. Dotted vectors are the offset between an (age, [M/H]) = (4.75 Gyr, 0.02) model and the Table 2 nuclear aperture observation. Solid vectors are the shifts predicted by considering a nonsolar pattern of [C/M]=+0.077, [N/M]=−0.13, [Mg/M]=−0.18, and [Na/M]=+0.12, as discussed in the text.

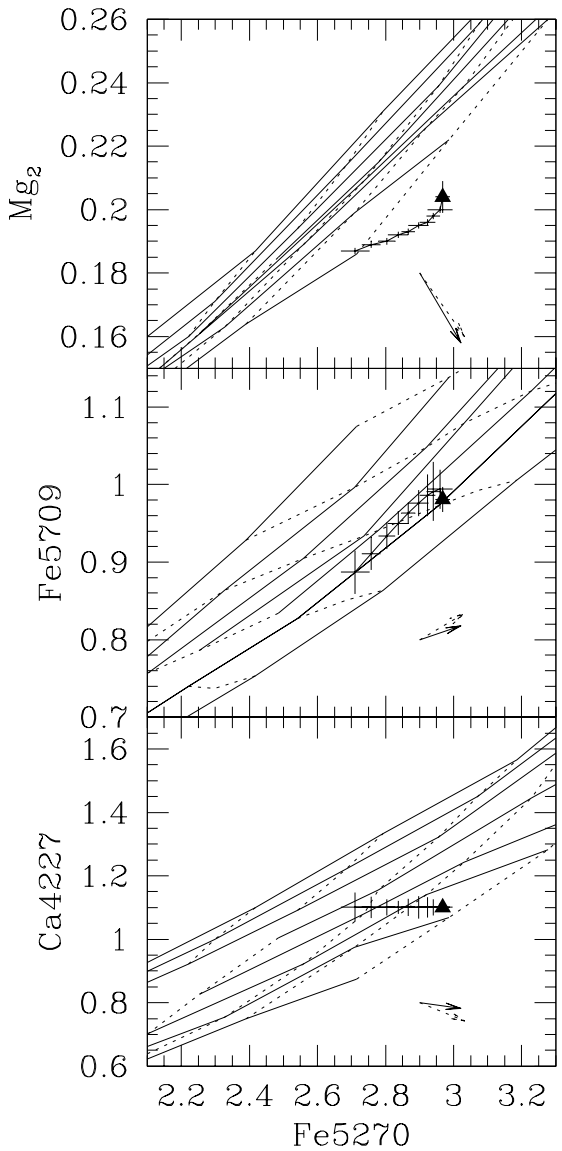

Fig. 6.— Index-index plots, with models and gradient data. Symbols are as in Figure 5.

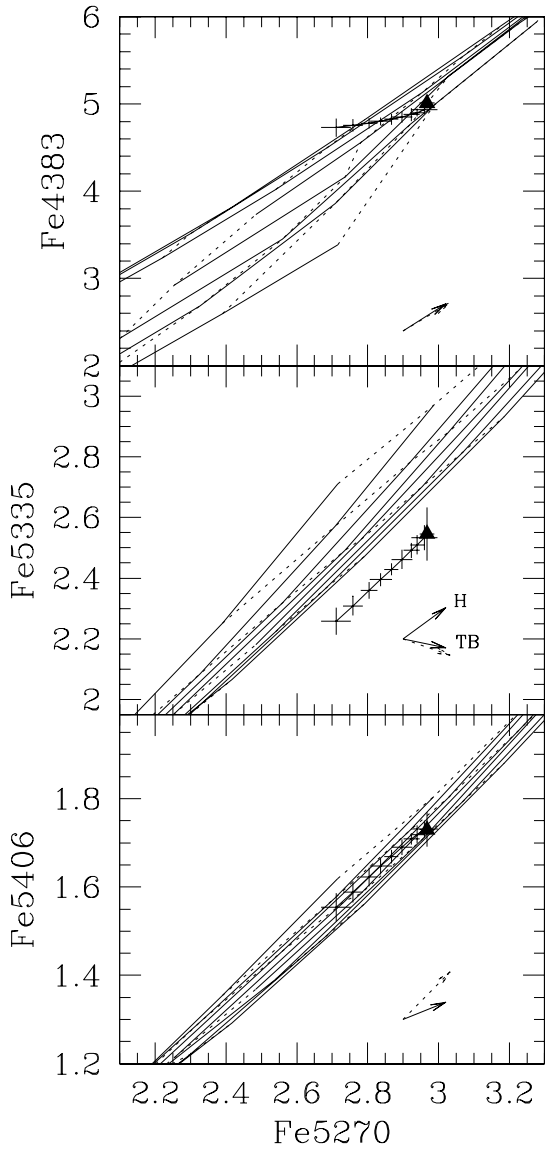

Fig. 7.— Index-index plots of abundance ratio effects. Symbols are as in Figure 5. The observations should overlay the model grid in these Fe-index vs. Fe-index diagrams if Fe were the sole driver in the feature strengths. The two solid vectors in the Fe5335 panel show different predictions from the synthetic spectra of TB95 vs. Houdashelt et al. (2002).

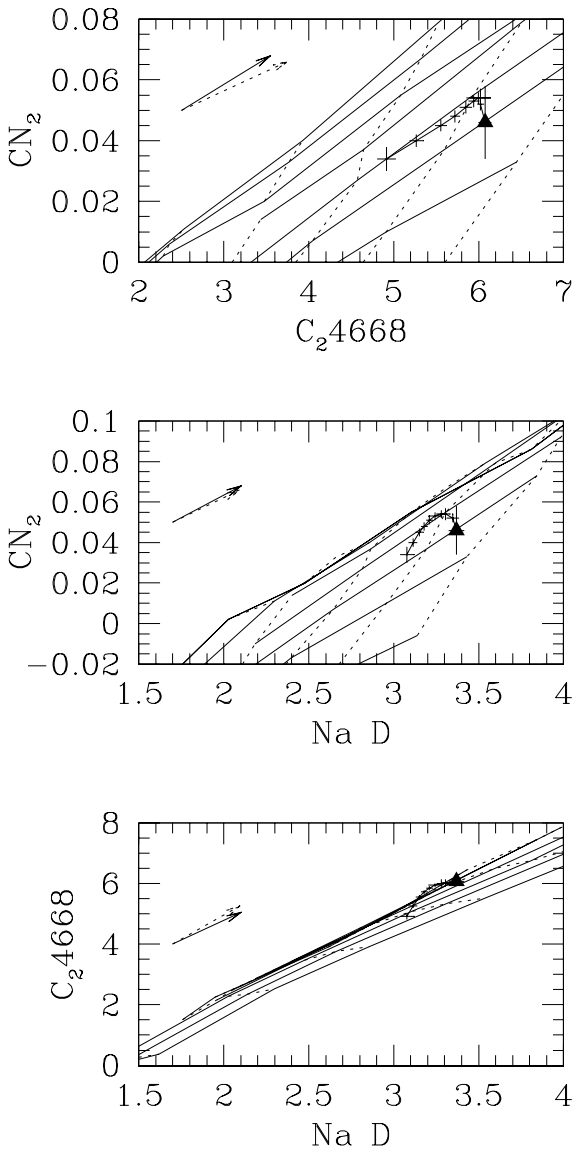

Fig. 8.— Index-index plots of the interplay between elements N, C, and Na. The CN index is affected by both the C and N abundances. Symbols are as in Figure 5.

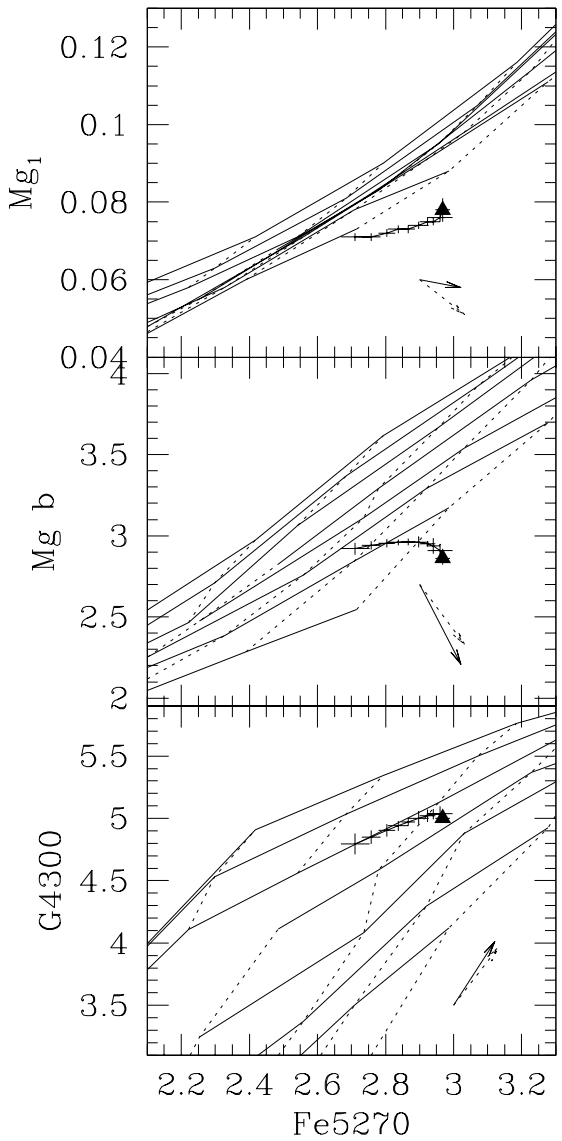

Fig. 9.— Index-index plots of the remaining Mg indices and G4300. G4300 gives an age nearly identical to that of the Balmer indices. None of the illustrated indices were used to iterate to the final age plus abundance-pattern solution. Symbols are as in Figure 5.

proved to be the best data set yet assembled by a comfortable margin. In the MDM data, random observational errors are much smaller than systematic errors.

The data reach slightly beyond 1 R_e along the major axis of M32, an angular distance of $44\farcs4$, or a physical distance of 164 pc. Only the CN indices show much evidence of nonmonotonic behavior by reaching a maximum about $4''$ from the nucleus and decreasing both toward the nucleus and away from it. This may indicate that the inner dozen pc of M32 are deficient in nitrogen, but confirming evidence is needed to be sure about this. The only other discontinuity present in M32, which has famously flat color gradients except in the ultraviolet, is in the surface brightness profile at $2''$ radius. No echo of this profile break is seen in stellar population indicators.

The mean age of the M32 nucleus, $\sim$4 Gyr, is consistent with other studies. The mean age increases with radius to 8−10 Gyr at 1 R_e. Correction for abundance ratios ages the nucleus to 4.7 Gyr. The nuclear abundance is slightly supersolar but fades rapidly to approximately [M/H]=−0.25 at 1 R_e. The differential radial trend is more certain than the zero point.

Different from almost every other elliptical galaxy, M32 has [Mg/Fe] subsolar in its dominant stellar population, about −0.18 dex. Other abundance results are [C/M]=+0.077, [N/M]=−0.13, [Fe/M]$\approx$0.0, and [Na/M]=+0.12. Other elements considered by TB95 do not show convincing evidence of enhancement: although the fit slightly preferred [Cr/M]= −0.15 and [Ti/M]= −0.2, these elements are consistent with [X/M]=0, along with O, Ca, and Si, because the Lick indices are not very sensitive to abundance changes in these elements.

Despite its astrophysical importance, oxygen cannot yet be measured. Given the fact that all of the various age diagnostic diagrams were splendidly self-consistent, oxygen is either near the solar ratio or its abundance is not important for the structure of metal-rich stars. If the former is true, then M32's abundance mixture is much closer to the solar neighborhood than that of giant elliptical galaxies. Nucleosynthetic theory has trouble predicting Na yields, but large portions of the N and C abundance are thought to come from mass loss in intermediate-mass stars. Using this as a handle, it seems simple enough to invent schemes in which the timing of winds or the presence of a black hole could alter the abundances of these common elements. Future work should replicate the suspicious CN index drop near the nucleus of M32. More flexible and internally consistent stellar population models of the type proposed in Worthey (1998) would solidify the age and abundance ratio results presented here.

The author gratefully acknowledges a suggestion from J. Kormendy to correlate the light profile of M32 with stellar population indicators and hopes he will forgive the negative result. J. J. González kindly provided his gradient data in electronic form. M. Houdashelt, M. Briley, E. Baron, and A. Kunth each separately provided synthetic spectra to confirm the TB95 overestimate of the effects of carbon. This work was supported by grant HF-1066.01-94A awarded by the Space Telescope Science Institute, which is operated by the Association of Universities for Research in Astronomy, Inc., for NASA under contract NAS5-26555; by Washington State University; and also

by the National Science Foundation under grant 0307487.

REFERENCES

Bender, R., Kormendy, J., & Dehnen, W. 1996, ApJ, 464, L123

Bender, R., & Surma, P. 1992, A&A, 258, 250

Bica, E. Alloin, D., & Schmidt, A. A., 1990, A&A, 228, 23

Burstein, D., Bertola, F., Buson, L. M., Faber, S. M., & Lauer, T. R. 1988, ApJ, 328, 440

Davidge, T. J., Robertis, M. M., & Yee, H. C. K. 1990, AJ, 100, 1143

Davidge, T. J. 1991, AJ, 101, 884

del Burgo, C., Peletier, R. F., Vazdekis, A., Arribas, S., & Mediavilla, E. 2001, MNRAS, 321, 227

de Vaucouleurs, G., de Vaucouleurs, A., Corwin, H. G., Jr., Buta, R. J., Paturel, G., & Fouqué, P. 1991, Third Reference Catalog of Bright Galaxies (New York: Springer)

González, J. J. 1993, Ph. D. Thesis, University of California, Santa Cruz (G93)

Grillmair, C. J., Lauer, T. R., Worthey, G., Faber, S. M., Freedman, W. L., Madore, B. F., Ajhar, E. A., Baum, W. A., Holtzman, J. A., Lynds, C. R., O'Neil, E. J. Jr., & Stetson, P. B. 1996, AJ, 112, 1975

Hardy, E., Couture, J., Couture, C., & Joncas, G. 1994, AJ, 107, 195

Houdashelt, M. L., Trager, S. C., Worthey, G., & Bell, R. A. 2002, BAAS, 201, 14.05

Jones, L. A., & Rose, J. A. 1994, BAAS, 184, 49.06

Kent, S. M. 1987, AJ, 94, 306

Kormendy, J. 1989, ApJ, 342, L63

Kormendy, J., & Bender, R. 1999, ApJ, 522, 772

Lauer, T. R., Faber, S. M., Ajhar, E. A., Grillmair, C. J., & Scowen, P. A. 1998, AJ, 116, 2263

O'Connell, R. W. 1980, ApJ, 236, 430

O'Connell, R. W., Martin, J. R., Crane, J. D., Sohn, S., Burstein, D., Bohlin, R. C., Landsman, W. B., Rood, R. T., & Wu, C.-C. 2000, BAAS, 197, 111.05

Rose, J. A. 1994, AJ, 107, 206

Tantalo, R., Chiosi, C., & Bressan, A. 1998, A&A, 333, 419

Thomas, D., & Maraston, C. 2003, A&A, 401, 429

Thomas, D., Maraston, C., & Bender, R. 2003, MNRAS, 339, 897

Trager, S. C., Faber, S. M., Worthey, G., & González, J. J. 2000, AJ, 119, 1645

Trager, S. C., Worthey, G., Faber, S. M., Burstein, D., & González, J. J. 1998, ApJS, 116, 1

Tripicco, M. J., & Bell, R. A. 1995, AJ, 110, 3035 (TB95)

Vazdekis, A., & Arimoto, N. 1999, ApJ, 525, 144

Worthey, G. 1994, ApJS, 95, 107

Worthey, G. 1998, PASP, 110, 888

Worthey, G., Faber, S. M., & González, J. J. 1992, ApJ, 398, 69

Worthey, G., Faber, S. M., González, J. J., & Burstein, D. 1994, ApJS, 94, 687

Worthey, G., & Ottaviani, D. L. 1997 ApJS, 111, 377

This preprint was prepared with the AAS LaTeX macros v5.2.

Table 2. Synthetic Circular-Aperture Indices and Errors

R/R_e	CN_1	CN_2	Ca4227	G4300	Fe4383	Ca4455	Fe4531	$C_2$4668	Hβ	Fe5015	Mg_1	Mg_2
0.1	0.021	0.053	1.101	5.021	4.902	1.624	3.416	6.002	2.199	5.256	0.075	0.198
	0.002	0.003	0.017	0.033	0.041	0.024	0.037	0.060	0.024	0.045	0.001	0.001
0.125	0.021	0.052	1.101	5.016	4.892	1.624	3.414	5.987	2.191	5.240	0.075	0.197
	0.002	0.002	0.019	0.035	0.045	0.026	0.038	0.062	0.026	0.053	0.001	0.001
0.25	0.020	0.051	1.101	4.991	4.860	1.624	3.399	5.904	2.156	5.188	0.074	0.195
	0.002	0.002	0.021	0.035	0.049	0.026	0.037	0.063	0.027	0.052	0.001	0.001
0.5	0.017	0.048	1.101	4.953	4.827	1.624	3.372	5.747	2.111	5.135	0.073	0.193
	0.002	0.002	0.023	0.041	0.054	0.027	0.042	0.065	0.027	0.051	0.001	0.001
1.0	0.013	0.045	1.101	4.909	4.798	1.624	3.339	5.526	2.063	5.088	0.072	0.191
	0.002	0.002	0.029	0.050	0.065	0.032	0.048	0.075	0.029	0.055	0.001	0.001
2.0	0.008	0.040	1.101	4.860	4.772	1.624	3.300	5.246	2.012	5.046	0.072	0.190
	0.003	0.004	0.038	0.070	0.088	0.042	0.058	0.095	0.034	0.071	0.001	0.001
R/Re	Mg b	Fe5270	Fe5335	Fe5406	Fe5709	Fe5782	Na D	TiO_1	Hδ_A	Hγ_A	Hδ_F	Hγ_F
0.1	2.933	2.933	2.503	1.713	0.986	0.875	3.300	0.038	-1.043	-4.309	0.678	-0.535
	0.024	0.019	0.029	0.015	0.017	0.016	0.024	0.002	0.052	0.040	0.031	0.019
0.125	2.937	2.925	2.494	1.708	0.983	0.871	3.289	0.038	-1.043	-4.303	0.668	-0.535
	0.024	0.020	0.028	0.015	0.017	0.016	0.025	0.002	0.058	0.042	0.032	0.021
0.25	2.947	2.895	2.460	1.688	0.972	0.857	3.251	0.038	-1.043	-4.284	0.636	-0.535
	0.022	0.022	0.026	0.016	0.016	0.016	0.023	0.002	0.060	0.042	0.033	0.022
0.5	2.949	2.856	2.417	1.660	0.956	0.839	3.209	0.039	-1.043	-4.264	0.603	-0.535
	0.023	0.024	0.026	0.018	0.017	0.016	0.023	0.002	0.065	0.050	0.037	0.027
1.0	2.943	2.815	2.372	1.630	0.937	0.820	3.171	0.039	-1.043	-4.247	0.575	-0.535
	0.026	0.028	0.030	0.021	0.019	0.019	0.027	0.002	0.081	0.064	0.047	0.034
2.0	2.930	2.772	2.325	1.598	0.915	0.800	3.135	0.039	-1.043	-4.231	0.549	-0.535
	0.032	0.036	0.039	0.027	0.024	0.025	0.035	0.003	0.108	0.079	0.062	0.044